

Localized Triplons and Site Stuffing in the Quantum Dimer Magnet BiYbGeO₅

Rachit Kapoor,^{1,*} D. R. Yahne,² V. O. Garlea,² and G. Hester^{1,†}

¹*Department of Physics, Brock University, St. Catharines, ON L2S 3A1, Canada.*

²*Neutron Scattering Division, Oak Ridge National Laboratory, Oak Ridge, TN 37831, USA.*

(Dated: May 30, 2025)

Thermodynamic and muon spin-relaxation measurements have recently highlighted BiYbGeO₅ as a new example of a rare-earth-based quantum dimer magnet with isolated Yb³⁺ spin- $\frac{1}{2}$ dimers. However, direct spectroscopic evidence of the triplet excitations and measurements of the structural disorder are lacking. In this work, polycrystalline BiYbGeO₅ was synthesized using conventional high-temperature solid-state methods and investigated via high-resolution neutron powder diffraction and inelastic neutron scattering. Diffraction measurements down to 58 mK reveal no signatures of magnetic order and indicate that nearly 20% of Yb³⁺ sites are replaced by non-magnetic Bi³⁺, introducing significant structural disorder. Inelastic neutron scattering shows dispersionless triplon excitations, consistent with localized, non-interacting spin dimers. Fits to the triplet excitation spectrum identify an XXZ-type anisotropic exchange with $J_{XX} = 0.11(2)$ meV and $J_Z = 0.15(1)$ meV. These findings establish BiYbGeO₅ as a structurally disordered but magnetically well-isolated quantum dimer system, providing a model platform for studying the resilience of entangled spin states to site dilution.

INTRODUCTION

Many exotic quantum states in condensed matter systems, such as quantum spin liquids, emerge from the entanglement of electron pairs into spin singlets. In a quantum spin liquid, the ground state can be described as a superposition of all possible singlet coverings of the lattice [1]. Understanding how singlets form and respond to perturbations is therefore essential for identifying and designing new quantum spin liquid candidates.

In cases where long-range entanglement is absent but local singlets form between neighboring spins without breaking lattice symmetries, the resulting state is known as a quantum dimer magnet. These systems are characterized by the absence of long-range magnetic order down to the lowest temperatures and the presence of coherent spin excitations – called triplons. In idealized models with negligible interdimer interactions, the singlet-triplet gap can be closed by an external magnetic field, leading directly to a fully polarized paramagnet. However, real materials invariably host finite interdimer interactions that can stabilize an intermediate field-induced phase, which maps onto a Bose-Einstein condensate of triplons [2]. Quantum dimer magnets thus serve as a minimal platform for exploring quantum entanglement and the onset of quantum criticality in low-dimensional spin systems.

To date, most quantum dimer magnets have been discovered in 3d transition metal-based compounds, where strong exchange interactions often result in prohibitively high magnetic field strengths (> 20 T) to close the single-triplet gap. The discovery of Yb₂Si₂O₇ in 2019 [4] marked the first rare-earth-based example of such a state, where the contracted nature of the 4f orbitals leads to a relatively small magnetic field to close the singlet-triplet gap (~1.0 T). Since the discovery of Yb₂Si₂O₇ several other 4f-based quantum magnets with emergent singlet ground states have been proposed in Yb₂SiO₅ [5], Yb-doped YAlO₃ [6], Yb₂Be₂SiO₇ [7], and BiYbGeO₅ [8].

BiYbGeO₅ is of particular interest as magnetometry, heat capacity, and muon spin relaxation measurements suggest the formation of isolated spin singlets composed of effective spin- $\frac{1}{2}$ Yb³⁺ moments [8]. Field-dependent heat capacity measurements by Mohanty *et al.* indicate anisotropic intradimer exchange with $J_{XX} \simeq 1.3$ K and $J_Z \simeq 2.6$ K with no thermodynamic evidence for interdimer interactions. These measurements confirm the absence of magnetic order at low tempera-

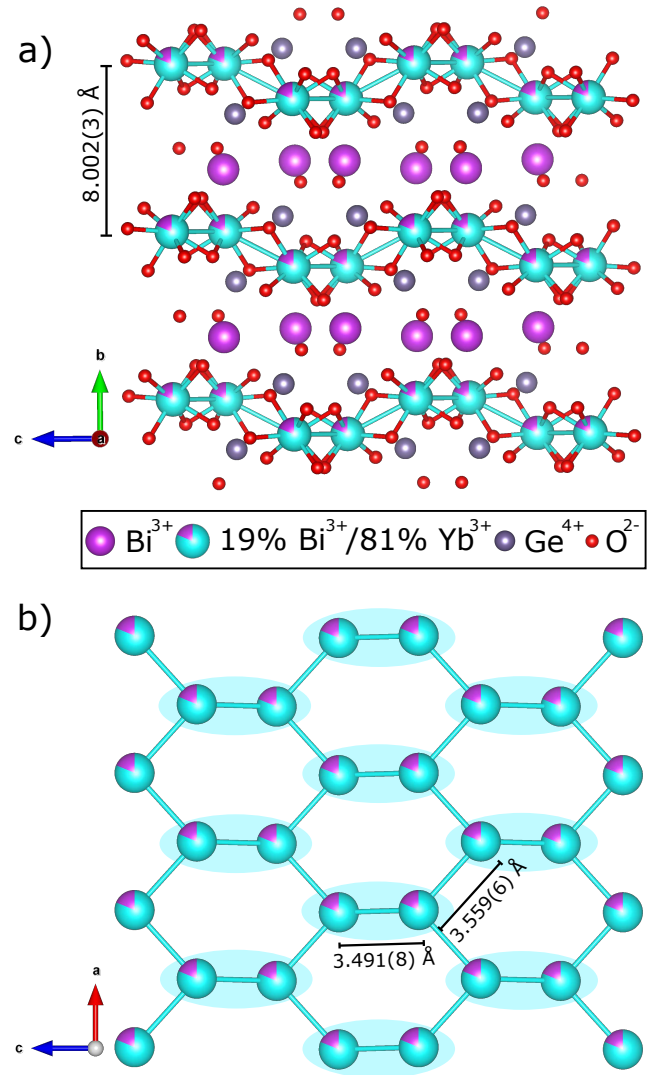


FIG. 1: a) Crystal structure of BiYbGeO₅ viewed along the a -axis [3]. The interlayer separation is 8.002(3) Å, which is considerably larger than the intradimer bond length of 3.491(8) Å. The fraction of Yb spheres shaded in the Bi color corresponds to the proposed amount (19.2(26)%) of Bi³⁺ stuffing at the Yb³⁺ site. b) The distorted honeycomb layers are viewed along the ac -plane with distortion along the b -axis. The dimers are labeled with blue ovals.

tures and the presence of ground state singlets; however, the

ideal method for confirming the presence of triplon excitations – and their energy scale – is inelastic neutron scattering, which has not been undertaken until this study.

In this work, we investigate the proposed dimer ground state in BiYbGeO_5 using inelastic neutron scattering to search for coherent triplon excitations and assess the degree of $\text{Bi}^{3+}/\text{Yb}^{3+}$ site disorder through high-resolution neutron diffraction. These measurements allow us to probe the strength of the intradimer and interdimer exchange and investigate how the triplon excitations survive in the presence of disorder, a key question for understanding the robustness of dimer physics beyond the clean limit.

EXPERIMENTAL METHODS

Synthesis

A pale-yellow polycrystalline powder of BiYbGeO_5 was synthesized using the solid-state synthesis method. This method is an adaptation from the synthesis method proposed by Cascales *et al.* [9]. Bi_2O_3 (99.99%, Thermo Scientific), Yb_2O_3 (99.9%, Sigma-Aldrich), and GeO_2 ($\geq 99.99\%$, Sigma-Aldrich) were dried to remove any water of crystallization, after which they were stored in a desiccator. Stoichiometric amounts of the dried reactants were taken in molar ratios of 1 : 1 : 2 in an agate mortar and pestle and ground, pressed into pellets, heated in air in an alumina crucible inside a box furnace for 24 hours each, and quenched [25]. This process was repeated four times, where the temperature was set to 800 °C, 900 °C, 950 °C, and 950 °C for each heating, respectively. For the last two heatings at 950 °C, the pellets were pressed by adding 1 ml of PVA (polyvinyl alcohol) solution (50 mg/ml) to facilitate proper pellet formation. Phase purity was assessed using powder X-ray diffraction (XRD) at room temperature using a Rigaku SmartLab X-ray Diffractometer (CuK_α source with $K_{\alpha 1}/K_{\alpha 2}$ of 1.540510Å/1.544330Å).

Neutron Powder Diffraction

Neutron diffraction measurements were performed on powdered BiYbGeO_5 using the HB-2A Neutron Powder Diffractometer (POWDER) at the High Flux Isotope Reactor at Oak Ridge National Laboratory and analyzed using the Rietveld refinement method within the FullProf Suite [10]. Approximately 5 g of the compound was loaded in a copper canister backfilled with 10 atm of He to ensure proper thermalization at low temperatures. Data was collected at 20 K, 0.9 K, and 0.058 K. Measurements were taken using two incident wavelengths of $\lambda = 2.41$ Å and $\lambda = 1.54$ Å using the Ge(113) and Ge (115) monochromators, respectively. For all measurements, the collimator setup was open-open-12'. A measurement with $\lambda = 1.54$ Å provided a larger Q range, allowing for more precise measurement of potential site mixing between Bi^{3+} and Yb^{3+} .

Inelastic Neutron Scattering

Inelastic neutron scattering (INS) spectra were measured at the Spallation Neutron Source at Oak Ridge National Laboratory using the BL-14B Hybrid Spectrometer (HYSPEC). Slices

and cuts of the data were made using the MANTID analysis software [11]. Data was collected at low temperature (0.250 K) to observe triplet excitations and at high temperature (100 K) as a background measurement. Multiple datasets were also collected at intermediary temperatures (0.580 K, 0.850 K, 1.5 K, 2.5 K, 10 K, and 20 K) to analyze the evolution of the triplet excitation intensity with increasing temperature. All measurements were performed under no external magnetic field in the unpolarized mode. The Fermi chopper speed was set at 420 Hz, and the lowest incident neutron energy of 3.8 meV was chosen to give the best possible resolution of $\Delta E \simeq 0.1$ meV at the elastic line. All data, except for 0.250 K, were collected using a detector bank covering a scattering angle (2θ) range of $8^\circ - 68^\circ$, giving horizontal detector coverage of 0.20 Å⁻¹ to 1.5 Å⁻¹ at the elastic line. To better measure the structure factor of the dimers at 250 mK, an extended detector coverage of $8^\circ - 95^\circ$ was used to give a $|Q|$ range of 0.20 Å⁻¹ to 2.0 Å⁻¹ at the elastic line.

RESULTS

Neutron Powder Diffraction

Refinement of the 20 K dataset yielded lattice parameters of $a = 5.2866(1)$ Å, $b = 15.1762(3)$ Å, and $c = 10.9333(2)$ Å, smaller than previously reported room-temperature values by Mohanty *et al.* [8] and Cascales *et al.* [9]. This contraction of the unit cell upon cooling is consistent with typical thermal contraction behavior.

Structural refinements of the $\lambda = 1.54$ Å scan at 20 K, further revealed a degree of site disorder between the Bi^{3+} and Yb^{3+} ions, likely driven by the similar ionic radii of Bi^{3+} (1.17 Å) and Yb^{3+} (0.985 Å) [12], their identical valence states, and that all atoms occupy the same Wyckoff position, imposing identical symmetry constraints. Approximately 19.2(26)% of the Yb^{3+} (occupying the Yb site, see Table I) are found to be replaced by Bi^{3+} , as determined by Rietveld analysis. Alternative scenarios, including Yb^{3+} occupancy of Bi^{3+} sites and bidirectional site mixing, were tested but yielded unrealistic parameters. Given that Bi^{3+} is non-magnetic, this substitution effectively breaks Yb-Yb magnetic dimers, generating an equivalent fraction of unpaired Yb^{3+} spins. Such site mixing defects are expected to locally increase the average interdimer distances and may play a crucial role in the low-temperature magnetic behavior of BiYbGeO_5 .

The absence of additional Bragg reflections across the entire measured temperature range confirms that all peaks are structural in origin, indicating a lack of long-range magnetic order down to 58 mK. To probe the possibility of short-range magnetic correlations, the diffraction pattern measured at 20 K was subtracted from the 0.058 K pattern. The resulting difference was featureless within the noise level, indicating the absence of any diffuse scattering and ruling out the presence of incipient magnetic transitions or short-range order.

Two temperature-independent impurity peaks are visible at $Q \approx 1.93$ Å⁻¹ and 2.11 Å⁻¹ with very small intensities. These peaks are not visible in the shorter-wavelength ($\lambda = 1.54$ Å) scan shown in Figure 2, likely due to reduced resolution at higher $|Q|$ values where peak overlap becomes more significant. The impurity peaks are visible in the longer wavelength neutron

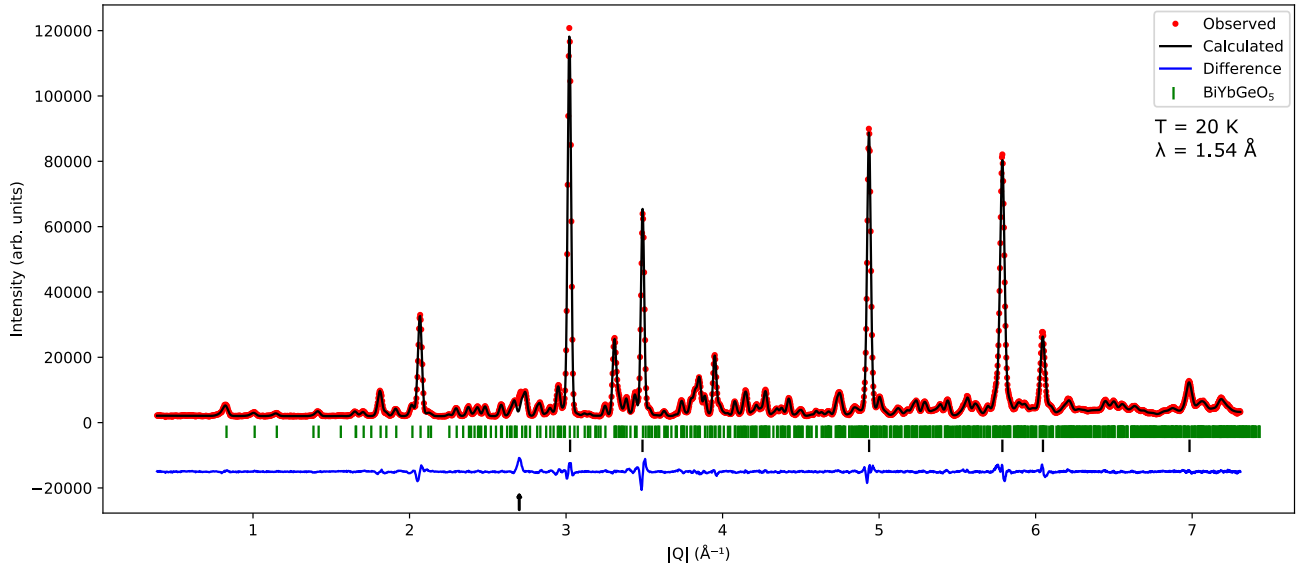


FIG. 2: A Rietveld refinement of the structure of BiYbGeO_5 obtained from neutron diffraction performed at 20 K using an incident wavelength of $\lambda = 1.54 \text{ \AA}$. The peaks, marked by black ticks, come from the Cu canister used for the measurement. These Cu peaks were fitted using Le Bail extraction, not to influence the refinement of the BiYbGeO_5 parameters. A spurious peak visible at $\sim 2.71 \text{ \AA}^{-1}$ (marked by a black arrow) corresponds to aluminum present in the sample environment due to inadequate collimation at 1.54 \AA incident wavelength. The overall χ^2 for the fit is 7.237.

scans and the XRD scan, which have been provided in the supplemental information [13].

Atom Site	x	y	z	B_{iso}	Occupancy
Bi1	8c 0.95685(69)	0.23741(24)	0.14649(38)	0.130(66)	1
Yb	8c 0.00808(65)	0.05396(15)	0.35944(30)	0.042(50)	0.808(26)
Bi2	8c 0.00808(65)	0.05396(15)	0.35944(30)	0.042(50)	0.192(26)
Ge	8c 0.00543(93)	0.40456(27)	0.40269(34)	0.282(62)	1
O1	8c 0.07054(97)	0.30183(32)	0.32959(48)	0.21(11)	1
O2	8c 0.3002(11)	0.43740(39)	0.45670(53)	0.19(8)	1
O3	8c 0.3182(14)	0.12552(40)	0.47399(56)	0.62(13)	1
O4	8c 0.2542(13)	0.15041(43)	0.23658(57)	0.50(10)	1
O5	8c 0.3493(11)	0.47814(43)	0.19261(54)	0.37(10)	1

TABLE I: The refined parameters of atomic coordinates (x , y , z), isotropic atomic displacement (B_{iso}), and site occupancy obtained by the Rietveld refinement of the neutron diffraction pattern of BiYbGeO_5 taken at 20 K using $\lambda = 1.54 \text{ \AA}$ incident wavelength.

Inelastic Neutron Scattering

To investigate the low-energy spin dynamics in BiYbGeO_5 , INS measurements were carried out using HYSPEC. As shown in Figures 3a-c, a well-defined excitation band is observed across a broad range of momentum transfers, $|Q|$. This excitation appears dispersionless within the instrumental resolution of $\sim 0.1 \text{ meV}$, consistent with isolated dimers with negligible interdimer exchange. Energy transfers were measured up to 3.61 meV (see supplemental information [13]), in which no crystalline electric field (CEF) excitations were detected, placing a lower bound on the CEF gap of 42 K.

The scattering intensity was plotted as a function of energy transfer (ΔE) by integrating a $|Q|$ range of $0.25 \text{ \AA}^{-1} - 1.4$

\AA^{-1} as shown in Figure 3d. Although the triplon excitation energy remains temperature-independent, its spectral weight decreases with increasing temperature, consistent with thermal depopulation of the singlet ground state.

To isolate the triplon excitation, the high-temperature (100 K) data were subtracted from the low-temperature (0.250 K) dataset, effectively removing the elastic background and sample environment. The resulting difference spectra show a single excitation that is limited by the instrument resolution. A two-Gaussian model was considered to estimate the intradimer exchange interactions, consistent with the expectations of an XXZ-type anisotropic exchange in isolated dimers. This model provided the best agreement with the INS data, as shown in Figure 4. Single and triple-Gaussian models were also tested, leading to poor and unrealistic fits, respectively. The single and triple-Gaussian fits, with their fitted parameters, have been included in the SI [13]. In order to more precisely determine the exchange interactions, a higher-resolution INS scattering experiment would be required.

In the XXZ dimer framework at zero magnetic field, three triplet excitations are expected: a single $S_z = 0$ state and a doubly degenerate excitation to the $S_z = \pm 1$ states, with the latter state expected to have a larger spectral weight. Under this assumption, the extracted exchange parameters were found to be $J_{XX} = 0.11(2) \text{ meV}$ and $J_Z = 0.15(1) \text{ meV}$, yielding an anisotropy ratio of $J_{XX}/J_Z \approx 0.73$. The energy hierarchy agrees qualitatively with that proposed by Mohanty *et al.* [8], which was inferred from heat capacity measurements. However, while the J_{XX} values are comparable within experimental uncertainty, the J_Z extracted from inelastic neutron scattering is significantly lower than previously reported. This discrepancy emphasizes the utility of direct spectroscopic probes such as INS for resolving anisotropic exchange strengths and may reflect inherent limitations of thermodynamic fitting approaches.

The Q -dependence of the triplet excitation at 0.250 K was further analyzed to confirm the spatial configuration of Yb dimers as shown in Figure 5. The measured intensity was fit to

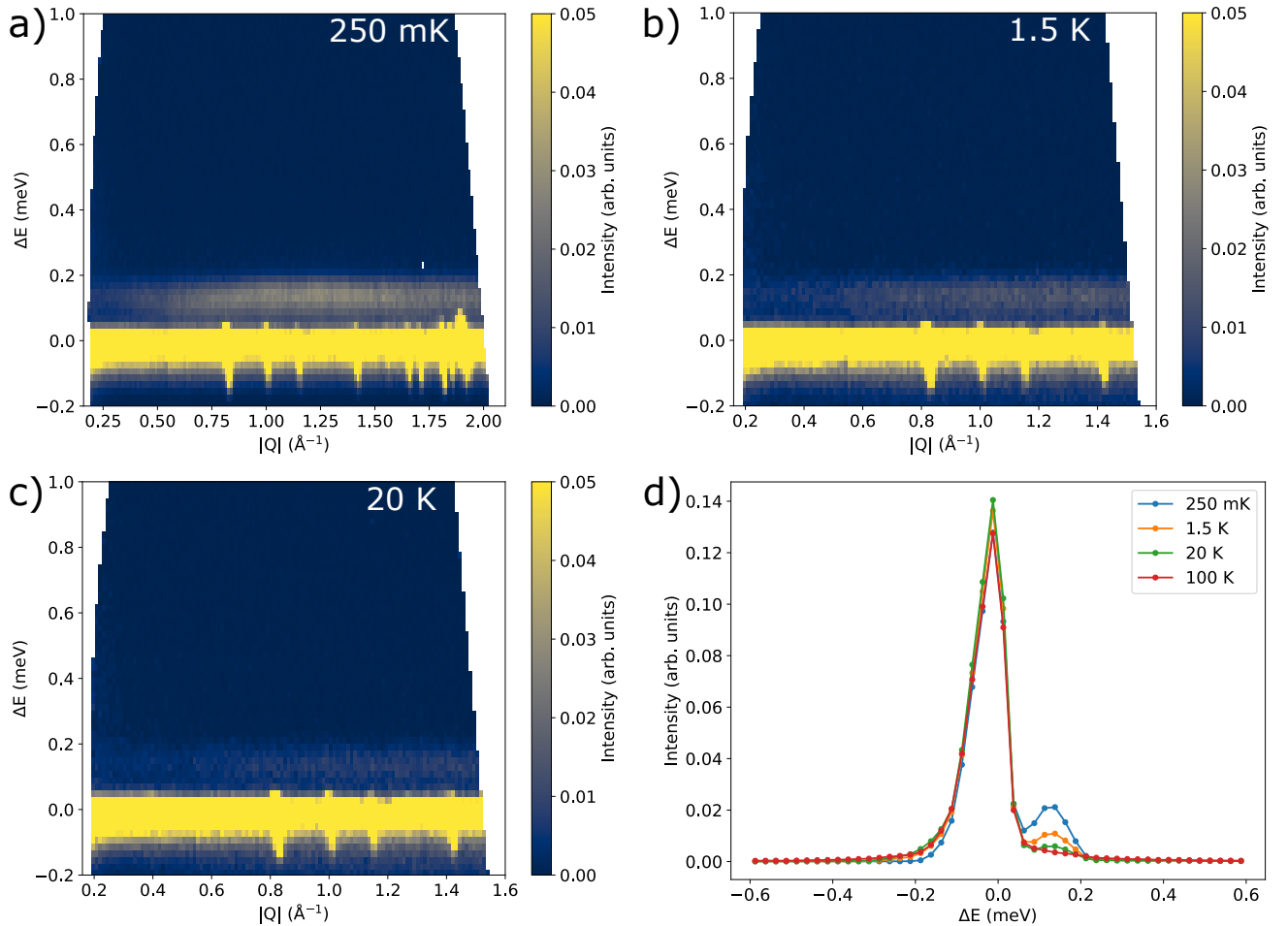


FIG. 3: a-c) ΔE vs $|Q|$ color contour slices of INS data at a) 250 mK, b) 1.5 K, and c) 20 K showing a flat triplon mode visible above the bright elastic line. The scale factor for all panels has been kept the same to show the triplon band getting fainter on increasing temperature, signifying the depopulation of the ground state. d) Cuts of the INS data made along ΔE integrating $|Q|$ from 0.25 \AA^{-1} to 1.4 \AA^{-1} for 250 mK, 1.5 K, and 20 K. The large peak at 0.0 meV is the elastic line. A temperature-dependent triplon mode is visible for all three temperatures.

Exchange interactions	This Work (meV)	Mohanty <i>et al.</i> (meV)
J_{XX}	0.11(2)	$\simeq 0.11$
J_Z	0.15(1)	$\simeq 0.22$

TABLE II: A comparison between the anisotropic exchange parameters measured in this work with INS and by Mohanty *et al.* by fitting heat capacity data [8].

the magnetic structure factor for an isolated dimer,

$$I(Q) = r_0^2 \frac{k'}{k} N p \times (f(Q))^2 \times \left(1 - \frac{\sin(Qd)}{Qd}\right)$$

where, $f(Q)$ is the magnetic form factor for Yb^{3+} and d is the intradimer distance. The magnetic form factor was modeled as $f(Q) = j_0 + \left(1 - \frac{g_s}{g}\right) j_2$ [14], using tabulated coefficients for Yb^{3+} [15]. The extracted dimer distance of $3.499(11) \text{ \AA}$ is in close agreement with the nearest-neighbor Yb-Yb spacing obtained from the Rietveld refinement of the neutron diffraction data collected at 58 mK ($3.495(9) \text{ \AA}$), confirming that the observed magnetic excitations originate from nearest-neighbor Yb dimers.

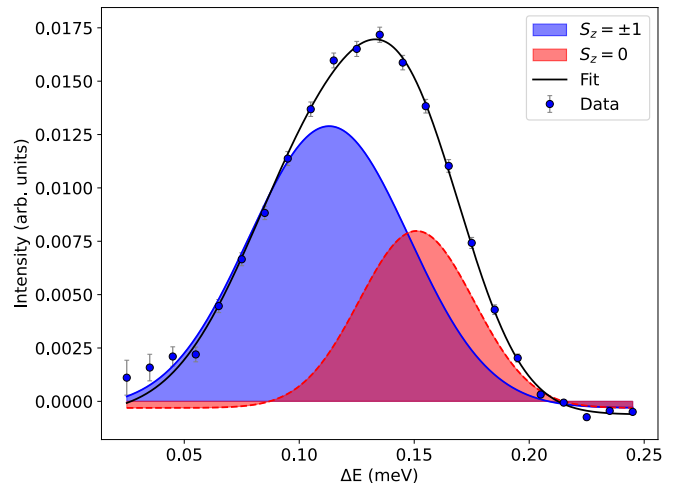


FIG. 4: A cut along ΔE made by subtracting the 100 K INS data from the 250 mK (integrating $|Q|$ from 0.25 \AA^{-1} to 1.4 \AA^{-1}). This excitation has been fit to the sum of two Gaussians, centered at $0.11(2) \text{ meV}$ and $0.15(1) \text{ meV}$, consistent with an XXZ-type intradimer exchange interaction. The full widths at half maximum for the Gaussians are 0.08 meV and 0.06 meV , respectively, which are smaller than the resolution of HYSPEC ($\sim 0.1 \text{ meV}$).

DISCUSSION

BiYbGeO₅ exhibits signatures of an isolated quantum dimer magnet, with a significant degree of Bi–Yb site mixing ($\simeq 19.2\%$) leading to broken Yb–Yb dimers. The substitution of non-magnetic Bi³⁺ for Yb³⁺ both increases the average separation between remaining magnetic dimers and may play a role in further suppressing interdimer triplon hopping, accounting for the flat band observed in inelastic neutron scattering. This level of site mixing occurs despite stoichiometric synthesis, implying that excess Bi³⁺ must occupy Yb³⁺ sites and expelled Yb³⁺ segregates into minor impurity phases. The number and intensity of these impurity peaks are too low to enable precise identification of the impurity phases. No signs of magnetic excitations from the impurity phase are observed in the inelastic neutron scattering data obtained from HYSPEC, likely due to the relatively small amount of impurity.

Previous work by Mohanty *et al.* [8] and Cascales *et al.* [9] utilized X-ray diffraction data of BiYbGeO₅ to assess phase purity and therefore they do not report any Yb/Bi site mixing. However, the x-ray cross-sections of Bi³⁺ (2.116×10^3 barns) and Yb³⁺ (1.454×10^3 barns) are fairly close, as that is predominantly a function of the number of electrons in the ions [16]. The neutron cross-sections, by contrast, are quite distinct (9.3148 barns for Bi and 19.42 barns for Yb), allowing one to discern the site mixing happening between the two ions [17]. The presence of site mixing is perhaps unsurprising as Cascales *et al.* also analyzed the XRD pattern of BiYGeO₅, which showed 12% of Bi³⁺ stuffing in the Y³⁺ site. In the work of Mohanty *et al.* they report an impurity contribution of $\simeq 4.2\%$ that is required to appropriately fit their field-dependent heat capacity data, assuming the impurity spin to be $S = 1/2$. The presence of this impurity may be explained by Bi³⁺ stuffing into the Yb³⁺ site where the substitution of a Yb–Yb dimer by a Bi–Yb pair results in an unpaired Yb³⁺ spin, which could yield this measured "impurity" contribution to magnetic susceptibility.

Site mixing effects of this sort are well known in Yb-based magnets and can dramatically alter magnetic behavior. For example, the pyrochlore quantum spin ice Yb₂Ti₂O₇ is notoriously sensitive to small off-stoichiometry. Even $\sim 2\%$ "stuffing" of the Ti⁴⁺ sites by extra Yb³⁺ leads to strongly sample-dependent ground states [18, 19]. Stoichiometric polycrystalline Yb₂Ti₂O₇ shows a sharp transition, whereas lightly stuffed single crystals exhibit broad heat-capacity anomalies and no conventional order [20]; demonstrating that magnetic properties can differ significantly between single crystals and polycrystalline samples due to subtle synthesis-dependent variations in disorder. By analogy, BiYbGeO₅'s site mixing similarly introduces random disruption, but in this case, the disorder further suppresses interdimer triplon hopping rather than creating competing couplings. Future growth of BiYbGeO₅ single crystals will be crucial to determine whether this site mixing is an intrinsic feature of the material or a consequence of polycrystalline synthesis.

Another instructive comparison is the Shastry–Sutherland, isolated dimer system Yb₂Be₂SiO₇. In this system, the site mixing between the non-magnetic Be²⁺ and Si⁴⁺ ions leads to a significant broadening of the triplon band as observed in INS measurements [7]. Er₂Be₂SiO₇, by contrast, does not show the Be/Si site mixing and develops long-range magnetic ordering

upon cooling [21]. Although the disorder in Yb₂Be₂SiO₇ is not at the magnetic site, it still perturbs the effective exchange landscape.

Beyond the experimental implications, the isolated dimers of BiYbGeO₅ may be an ideal system for testing quantum simulations of entangled states in condensed matter systems. Quantum dimer magnets serve as an ideal two-qubit prototype for quantum simulation, directly mapping each spin in a dimer to a qubit pair and encoding the antiferromagnetic exchange interaction into entangling gates [22, 23]. Eassa *et al.* demonstrated that resource-efficient fast-forwarding measurement performed with short-depth circuits can faithfully reproduce the dynamical structure factor and the triplon gap of dimers on current quantum processors, with fidelities high enough to match costly INS measurements [24]. BiYbGeO₅ may be an ideal system for extending that analysis to rare-earth-based quantum magnets.

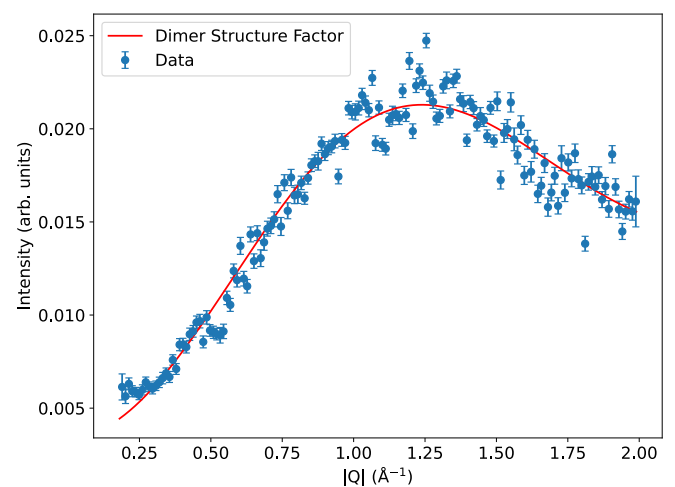


FIG. 5: A cut of the INS data taken at 250 mK made along $|Q|$ by integrating ΔE from 0.09 meV to 0.20 meV. The fitted line represents the calculated structure factor of a dimer magnet system that yields an intradimer distance of 3.499(11) Å.

CONCLUSIONS

In this work, polycrystalline samples of BiYbGeO₅ were synthesized via conventional solid-state reactions, and their magnetic and structural properties were investigated through neutron powder diffraction and inelastic neutron scattering. Neutron diffraction measurements carried out at 20 K, 0.9 K, and 58 mK, confirming the absence of magnetic orderings. Structural refinements revealed significant site disorder, with 19.2(26)% of Yb³⁺ sites replaced by non-magnetic Bi³⁺ ions. Inelastic neutron scattering measurements uncovered dispersionless triplon excitations, consistent with localized triplet modes due to isolated Yb–Yb dimers. Gaussian fits to the energy spectrum yielded an XXZ-type anisotropic exchange interaction, with $J_{XX} = 0.11(2)$ meV and $J_Z = 0.15(1)$ meV. Analysis of the magnetic structure factor further determined the intradimer Yb–Yb distance to be 3.499(11) Å, in excellent agreement with the nearest-neighbor spacing extracted from diffraction. These results confirm that despite substantial structural disorder, BiYbGeO₅ hosts a magnetically disordered quantum ground state composed of well-isolated Yb dimers,

making it a compelling platform for exploring disorder-resilient quantum magnetism.

ACKNOWLEDGEMENTS

R. Kapoor and G. Hester would like to thank R. Ganesh for insightful conversations closely and distantly related to this work. We would also like to thank C. Sarkis for facilitating the measurements using HYSPEC for this work. We also extend our gratitude to Carter Fortuna for synthesizing many variants of this material. A portion of this work used resources at the High-Flux Isotope Reactor and the Spallation Neutron Source, which are DOE Office of Science User Facilities operated by Oak Ridge National Laboratory. The beamtime was allocated to POWDER (HB-2A) and HYSPEC (BL-14B) on proposal numbers IPTS-32979 and IPTS-35019, respectively.

* Electronic address: ls23aj@brocku.ca

† Electronic address: ghester@brocku.ca

- [1] L. Balents, *Nature* **464**, 199 (2010).
- [2] V. Zapf, M. Jaime, and C. Batista, *Reviews of Modern Physics* **86**, 563 (2014).
- [3] K. Momma and F. Izumi, *International Union of Crystallography* **44**, 1272 (2011).
- [4] G. Hester, H. Nair, T. Reeder, D. Yahne, T. DeLazzer, L. Berges, D. Ziat, J. Neilson, A. Aczel, G. Sala, et al., *Physical Review Letters* **123**, 027201 (2019).
- [5] M. Hase, K. Kaneko, C. Tabata, H. Yamauchi, N. Tsujii, and A. Dönni, *Physical Review B* **111**, 094403 (2025).
- [6] S. E. Nikitin, T. Xie, A. Podlesnyak, and I. A. Zaliznyak, *Physical Review B* **101**, 245150 (2020).
- [7] A. Brassington, Q. Ma, G. Duan, S. Calder, A. I. Kolesnikov, K. M. Taddei, G. Sala, H. Wang, W. Xie, B. A. Frandsen, et al. (2025), [arXiv:2505.00766 \[cond-mat\]](https://arxiv.org/abs/2505.00766).
- [8] S. Mohanty, S. S. Islam, N. Winterhalter-Stocker, A. Jesche, G. Simutis, C. Wang, Z. Guguchia, J. Sichelschmidt, M. Baenitz, A. A. Tsirlin, et al., *Physical Review B* **108**, 134408 (2023).
- [9] C. Cascales, J. Antonio Campa, E. Gutiérrez Puebla, M. Angeles Monge, C. Ruíz Valero, and I. Rasines, *Journal of Materials Chemistry* **12**, 3626 (2002).
- [10] J. Rodríguez-Carvajal, *Physica B: Condensed Matter* **192**, 55 (1993).
- [11] O. Arnold, J.-C. Bilheux, J. Borreguero, A. Buts, S. I. Campbell, L. Chapon, M. Doucet, N. Draper, R. F. Leal, M. Gigg, et al., *Nuclear instruments and methods in physics research section a: accelerators, spectrometers, detectors and associated equipment* **764**, 156 (2014).
- [12] R. D. Shannon, *International Union of Crystallography* **32**, 751 (1976).
- [13] *See Supplemental Information for additional neutron diffraction data, inelastic scattering spectra, fits to the triplet excitations, and x-ray diffraction data.*
- [14] S. W. Lovesey and J. W. Lynn, *Theory of Neutron Scattering from Condensed Matter, Volume 1 and 2*, vol. 39 (1986).
- [15] A. Freeman and J. Desclaux, *Journal of Magnetism and Magnetic Materials* **12**, 11 (1979).
- [16] S. Seltzer, (No Title) (1987).
- [17] F. S. Varley, *Neutron news* **3**, 29 (1992).
- [18] J. Gaudet, D. D. Maharaj, G. Sala, E. Kermarrec, K. A. Ross, H. A. Dabkowska, A. I. Kolesnikov, G. E. Granroth, and B. D. Gaulin, *Physical Review B* **92**, 134420 (2015).
- [19] S. S. Ghosh and E. Manousakis, *Physical Review B* **97**, 245117 (2018).
- [20] K. A. Ross, T. Proffen, H. A. Dabkowska, J. A. Quilliam, L. R. Yaraskavitch, J. B. Kycia, and B. D. Gaulin, *Physical Review B* **86**, 174424 (2012).
- [21] A. Brassington, Q. Ma, G. Sala, A. I. Kolesnikov, K. M. Taddei, Y. Wu, E. S. Choi, H. Wang, W. Xie, J. Ma, et al. (2024), [arXiv:2405.08230 \[cond-mat\]](https://arxiv.org/abs/2405.08230).
- [22] A. Ardavan, A. M. Bowen, A. Fernandez, A. J. Fielding, D. Kaminski, F. Moro, C. A. Muryn, M. D. Wise, A. Ruggi, E. J. L. McInnes, et al., *npj Quantum Information* **1**, 15012 (2015).
- [23] H. Jing-Min, T. Li-Jun, and G. Mo-Lin, *Chinese Physics Letters* **22**, 2147 (2005).
- [24] N. M. Eassa, J. Gibbs, Z. Holmes, A. Sornborger, L. Cincio, G. Hester, P. Kairys, M. Motta, J. Cohn, and A. Banerjee, *Physical Review B* **110**, 184414 (2024).
- [25] It was found with further synthesis that quenching is not necessary and the pellets can be cooled at a slower rate as well

SUPPLEMENTARY INFORMATION

Localized Triplons and Site-Stuffing in the Quantum Dimer Magnet BiYbGeO_5

Rachit Kapoor,^{1,*} D. R. Yahne,² V. O. Garlea,² and G. Hester^{1,†}

¹*Department of Physics, Brock University, St. Catharines, ON L2S 3A1, Canada.*

²*Neutron Scattering Division, Oak Ridge National Laboratory, Oak Ridge, TN 37831, USA.*

(Dated: May 30, 2025)

X-RAY DIFFRACTION

The XRD pattern shows three additional impurity peaks at $|\vec{Q}| = 1.86 \text{ \AA}^{-1}$, 1.93 \AA^{-1} , and 2.10 \AA^{-1} . The intensity of the peaks is weak with normalized intensities of 0.04, 0.03, and 0.04, respectively. The peak seen at 1.86 \AA^{-1} is only visible in the XRD pattern but is invisible in all neutron powder diffraction (NPD) scans. The number and intensity of these impurity peaks are too low to enable precise identification of the impurity phase(s).

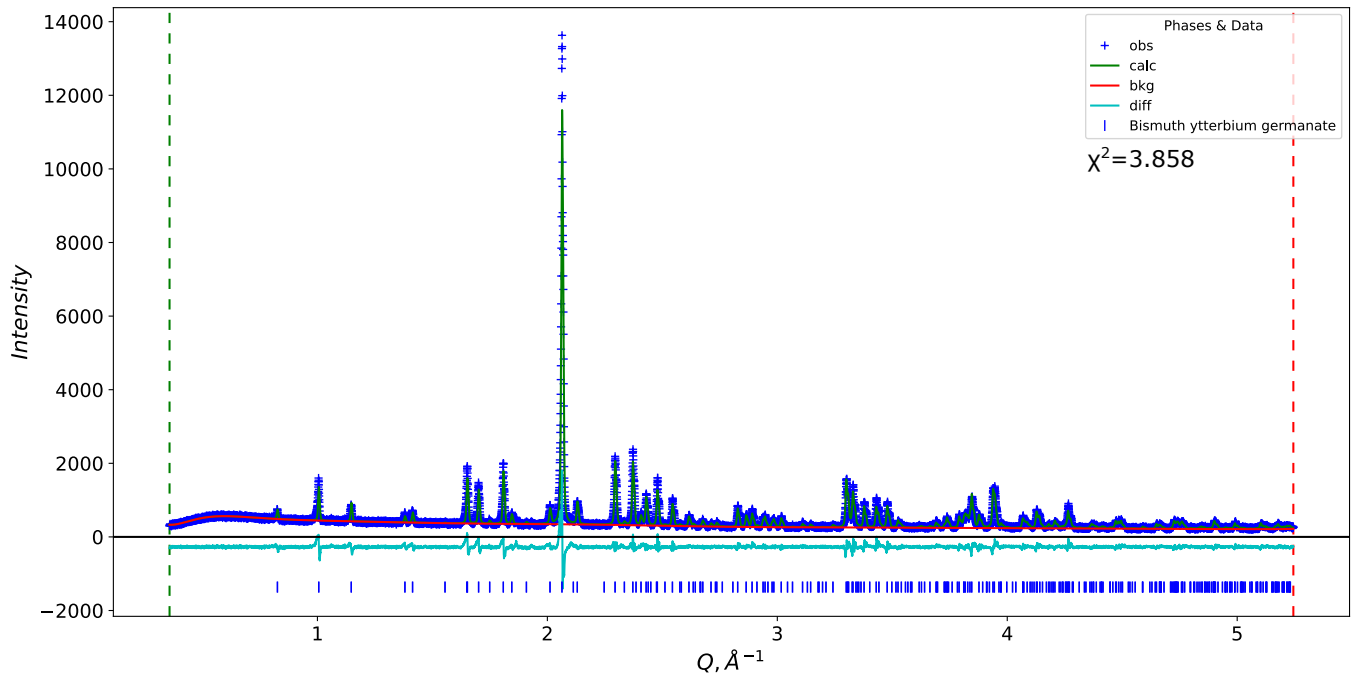


FIG. 1: A Rietveld refinement of the structure of BiYbGeO_5 obtained from X-ray diffraction performed at room temperature using a Rigaku SmartLab X-ray Diffractometer (CuK_α source with $\text{K}_{\alpha 1}/\text{K}_{\alpha 2}$ wavelength of $1.540510\text{\AA}/1.544330\text{\AA}$).

NEUTRON POWDER DIFFRACTION

Neutron diffraction measurements performed at 20 K using 1.54 Å incident wavelength show an unindexed peak visible in the pattern at 2.71 \AA^{-1} . This peak is not visible in any of the neutron diffraction patterns using the longer incident wavelengths or the XRD pattern. The other three scans were performed with an incident wavelength of 2.41 Å. Two additional peaks at $Q \approx 1.93 \text{ \AA}^{-1}$ and 2.11 \AA^{-1} were detected at all temperatures with very small intensities.

The lattice parameters obtained for each scan type are given in Table I. For the refinement of these patterns, the isotropic atomic displacement (B_{iso}) was refined only for the 1.54 Å scan because the peaks at higher $|Q|$ are more sensitive to this parameter. Since high $|Q|$ data was not possible for 2.71 \AA^{-1} , B_{iso} values were kept at their original values as given by the crystallographic information file [?].

Temperature (Incident Wavelength)	a	b	c
20 K (1.54 Å)	5.2866(1)	15.1762(3)	10.9333(2)
20 K (2.41 Å)	5.2851(1)	15.1720(3)	10.9252(2)
900 mK (2.41 Å)	5.2853(1)	15.1728(3)	10.9258(2)
50 mK (2.41 Å)	5.2849(1)	15.1719(3)	10.9250(2)

TABLE I: Lattice parameters a , b , c (in Å) as given by refining different sets of neutron diffraction.

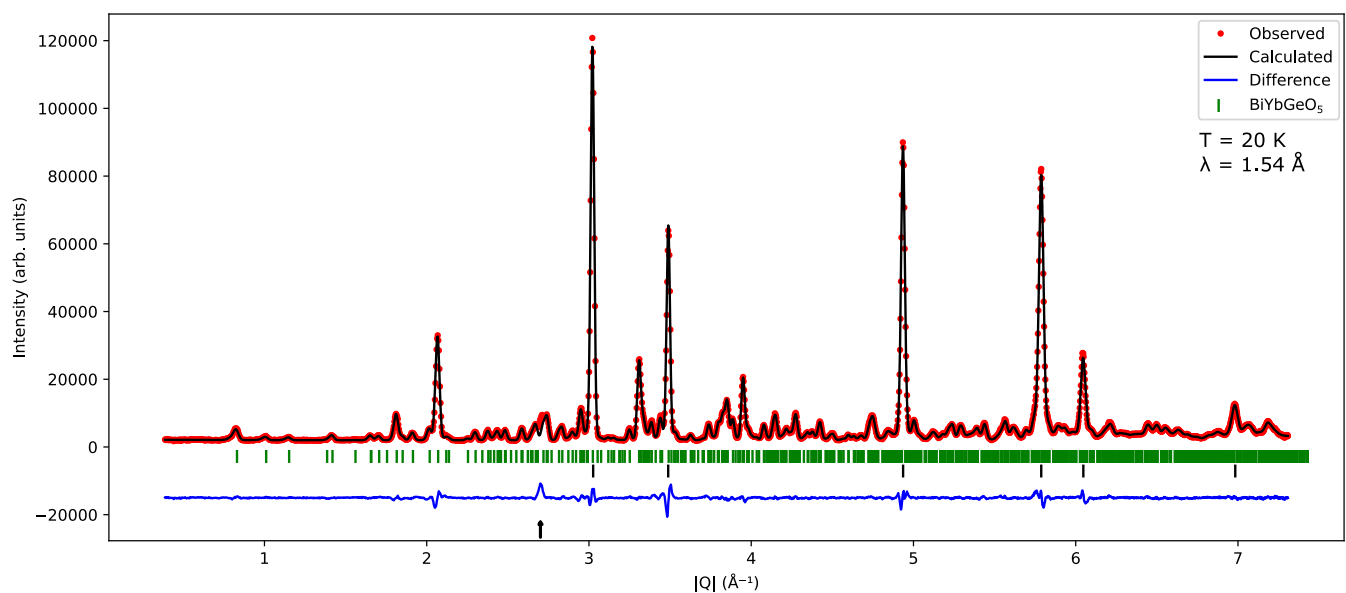


FIG. 2: A Rietveld refinement of the structure of BiYbGeO_5 obtained from neutron diffraction performed at 20 K using an incident wavelength of $\lambda = 1.54 \text{ \AA}$. The peaks, marked by black arrows, come from the Cu canister used for the measurement. These Cu peaks were fitted using Le Bail extraction, not to influence the refinement of the BiYbGeO_5 parameters. The R_{bragg} for the pattern from BiYbGeO_5 is 3.94 ($\chi^2 = 7.20$).

Atom Site		x	y	z	B_{iso}	Occupancy
Bi1	8c	0.95685(69)	0.23741(24)	0.14649(38)	0.130(66)	1
Yb	8c	0.00808(65)	0.05396(15)	0.35944(30)	0.042(50)	0.808(26)
Bi2	8c	0.00808(65)	0.05396(15)	0.35944(30)	0.042(50)	0.192(26)
Ge	8c	0.00543(93)	0.40456(27)	0.40269(34)	0.282(62)	1
O1	8c	0.07054(97)	0.30183(32)	0.32959(48)	0.21(11)	1
O2	8c	0.3002(11)	0.43740(39)	0.45670(53)	0.19(8)	1
O3	8c	0.3182(14)	0.12552(40)	0.47399(56)	0.62(13)	1
O4	8c	0.2542(13)	0.15041(43)	0.23658(57)	0.50(10)	1
O5	8c	0.3493(11)	0.47814(43)	0.19261(54)	0.37(10)	1

TABLE II: The refined parameters of atomic coordinates (x , y , z), isotropic atomic displacement (B_{iso}), and site occupancy ($Occupancy$) obtained by the Rietveld refinement of the neutron diffraction pattern of BiYbGeO₅ taken at 20 K using $\lambda = 1.54 \text{ \AA}$ incident wavelength.

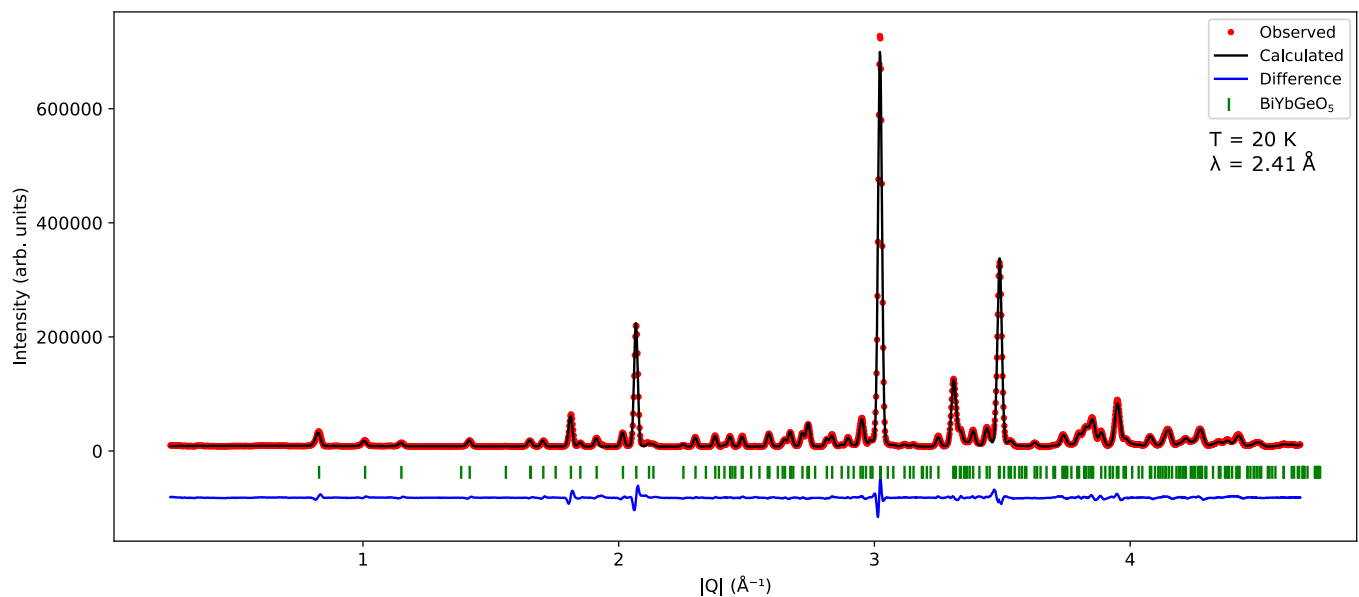


FIG. 3: A Rietveld refinement of the structure of BiYbGeO₅ obtained from neutron diffraction performed at 20 K using an incident wavelength of $\lambda = 2.41 \text{ \AA}$. The peaks at 3.02 \AA and 3.49 \AA , come from the Cu canister used for the measurement. These Cu peaks were fitted using Le Bail extraction, not to influence the refinement of the BiYbGeO₅ parameters. The R_{bragg} for the pattern from BiYbGeO₅ is 4.25 ($\chi^2 = 32.71$).

INELASTIC NEUTRON SCATTERING

ΔE vs $|Q|$ Full Range Slice

Figure 6 shows the full range of the INS data collected at 250 mK. It shows a bright band at the elastic line and a flat triplon band. The energy transfer range goes from -7.59 meV to 3.61 meV , in which no crystalline electric field (CEF) excitations were detected, placing a lower bound on the CEF gap of 42 K.

Gaussian Fits of $I(\Delta E)$ Cuts of Inelastic Neutron Scattering

Gaussians were given by:

$$I(\Delta E) = H + ae^{-\left(\frac{(\Delta E - b)^2}{2c^2}\right)}$$

where,

H is the baseline for the curve

a is the amplitude of the Gaussian

Atom	Site	x	y	z	B_{iso}	Occupancy
Bi1	8c	0.96058(87)	0.23660(30)	0.14542(46)	0.35791	1
Yb1	8c	0.00784(78)	0.05417(18)	0.35858(42)	0.11052	0.808(23)
Bi2	8c	0.00784(78)	0.05417(18)	0.35858(42)	0.11052	0.192(23)
Ge1	8c	0.0108(13)	0.40507(30)	0.40302(37)	0.36060	1
O1	8c	0.0671(11)	0.30050(43)	0.33105(60)	0.41847	1
O2	8c	0.2991(16)	0.43892(43)	0.45977(75)	0.60797	1
O3	8c	0.3085(15)	0.12600(46)	0.47115(57)	0.44216	1
O4	8c	0.2546(18)	0.15159(48)	0.23504(64)	0.35531	1
O5	8c	0.3541(13)	0.47897(57)	0.19456(64)	0.43426	1

TABLE III: The refined parameters of atomic coordinates (x , y , z), and site occupancy (*Occupancy*) obtained by the Rietveld refinement of the neutron diffraction pattern of BiYbGeO₅ taken at 20 K using $\lambda = 2.41$ Å incident wavelength.

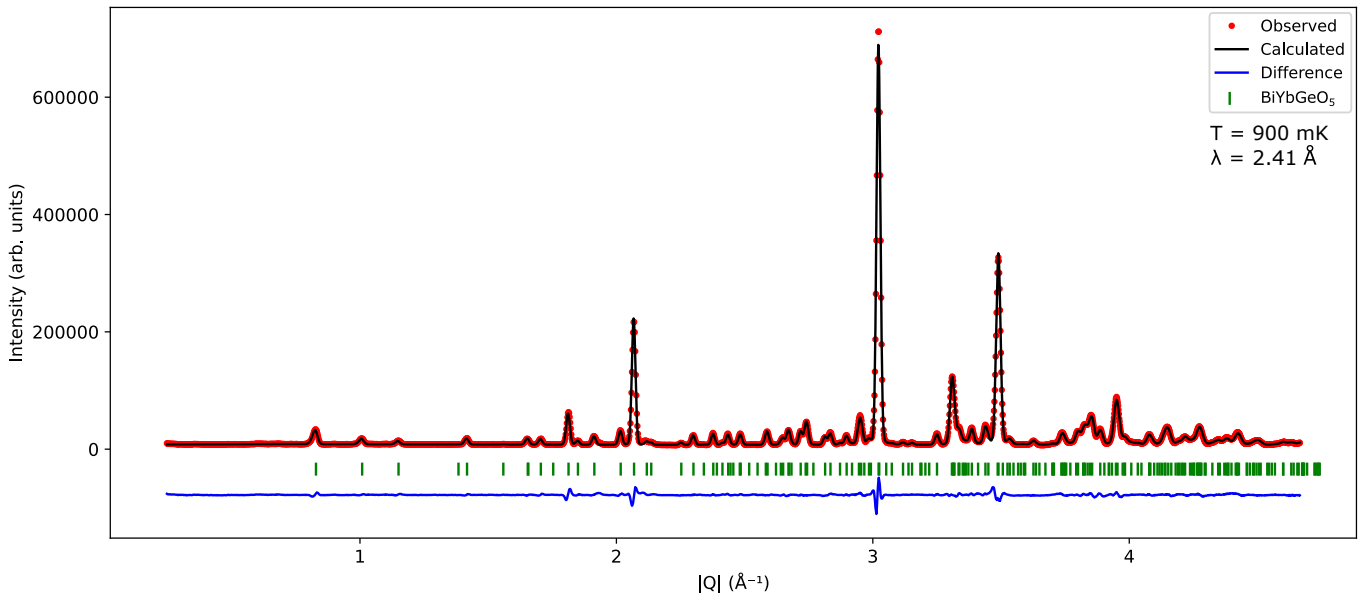


FIG. 4: A Rietveld refinement of the structure of BiYbGeO₅ obtained from neutron diffraction performed at 900 mK using an incident wavelength of $\lambda = 2.41$ Å. The peaks at 3.02 Å and 3.49 Å, come from the Cu canister used for the measurement. These Cu peaks were fitted using Le Bail extraction, not to influence the refinement of the BiYbGeO₅ parameters. The R_{bragg} for the pattern from BiYbGeO₅ is 4.18 ($\chi^2 = 27.37$).

b is the center of the Gaussian

c is the standard deviation or the Gaussian RMS

$$\text{FWHM} = \sqrt{2 \ln 2} \cdot c \approx 2.355c$$

A single Gaussian fit would suggest a Heisenberg interaction where the triplet excitation is triply degenerate. As the resolution of the instrument limits the triplon excitation observed. Attempts to fit the excitation to a single-Gaussian model yielded a full-width at half-maximum (FWHM) comparable to the instrument's resolution (see Figure 7). This fit has a high χ^2 value of 128.688, indicating a poor fit. The fitted parameters are given in Table VI.

A double Gaussian model would suggest an XXZ interaction such that $S_z = \pm 1$ states are doubly degenerate and $S_z = 0$ has a separate energy. This fit has a χ^2 value of 25.382 (see Figure 8). The fitted parameters are given in Table VII.

A triple Gaussian model would mean an XYZ interaction such that $S_z = +1$, $S_z = -1$, and $S_z = 0$ all have different energies. This leads to a better fit, as expected, based on the increase in the number of refined parameters. The triplon peak 3 (shown in red in Figure 9) has very large error margins, and the FWHM exceeds the resolution of the instrument itself. The peak is close to the elastic line and appears due to imperfect subtraction.

Atom	Site	x	y	z	B_{iso}	Occupancy
Bi1	8c	0.96037(81)	0.23650(28)	0.14556(43)	0.35791	1
Yb	8c	0.00872(71)	0.05410(16)	0.35890(38)	0.11052	0.836(21)
Bi2	8c	0.00872(71)	0.05410(16)	0.35890(38)	0.11052	0.164(21)
Ge	8c	0.0100(12)	0.40471(28)	0.40304(34)	0.36060	1
O1	8c	0.0660(10)	0.30066(40)	0.33116(55)	0.41847	1
O2	8c	0.2980(14)	0.43935(40)	0.45988(69)	0.60797	1
O3	8c	0.3085(14)	0.12618(43)	0.47156(52)	0.44216	1
O4	8c	0.2547(16)	0.15185(44)	0.23509(59)	0.35531	1
O5	8c	0.3553(12)	0.47932(52)	0.19390(59)	0.43426	1

TABLE IV: The refined parameters of atomic coordinates (x , y , z), and site occupancy (*Occupancy*) obtained by the Rietveld refinement of the neutron diffraction pattern of BiYbGeO₅ taken at 900 mK using $\lambda = 2.41$ Å incident wavelength.

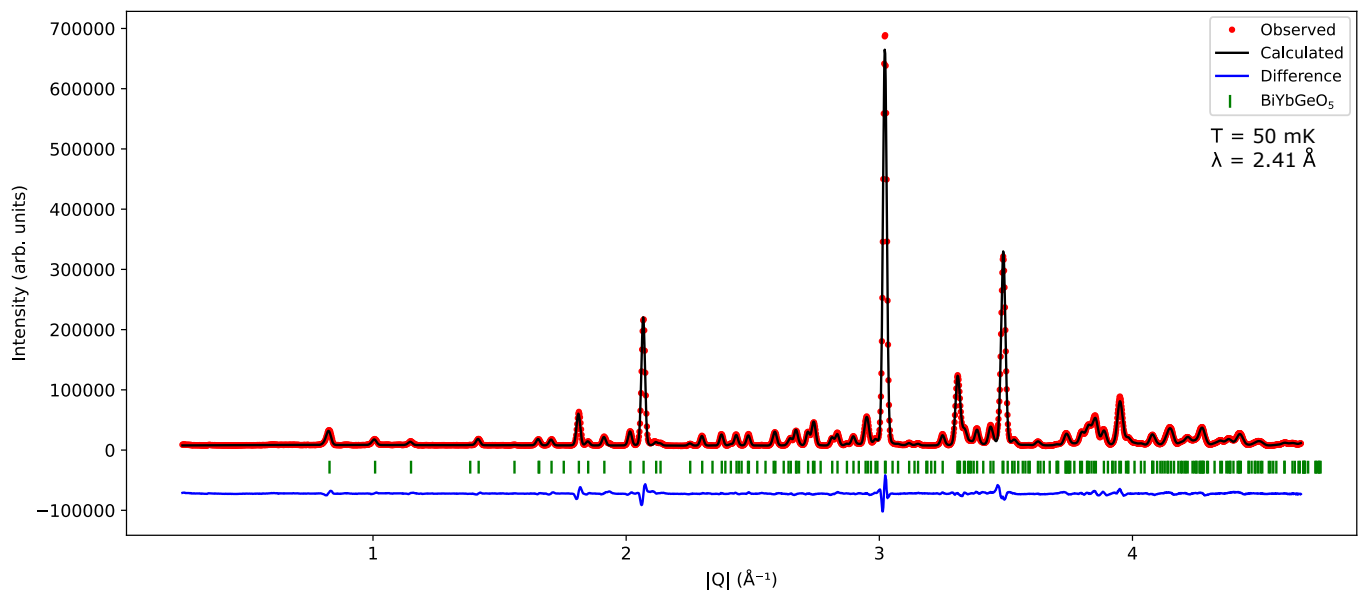


FIG. 5: A Rietveld refinement of the structure of BiYbGeO₅ obtained from neutron diffraction performed at 50 mK using an incident wavelength of $\lambda = 2.41$ Å. The peaks at 3.02 Å and 3.49 Å, come from the Cu canister used for the measurement. These Cu peaks were fitted using Le Bail extraction, not to influence the refinement of the BiYbGeO₅ parameters. The R_{bragg} for the pattern from BiYbGeO₅ is 4.32 ($\chi^2 = 29.05$).

* Electronic address: ls23aj@brocku.ca

† Electronic address: ghester@brocku.ca

Atom	Site	x	y	z	B_{iso}	Occupancy
Bi1	8c	0.96081(84)	0.23679(29)	0.14580(44)	0.35791	1
Yb	8c	0.00870(74)	0.05415(17)	0.35891(40)	0.11052	0.821(22)
Bi2	8c	0.00870(74)	0.05415(17)	0.35891(40)	0.11052	0.179(22)
Ge1	8c	0.0108(13)	0.40476(29)	0.40273(35)	0.36060	1
O1	8c	0.0671(10)	0.30060(41)	0.33119(57)	0.41847	1
O2	8c	0.2985(15)	0.43949(41)	0.46045(71)	0.60797	1
O3	8c	0.3083(14)	0.12617(44)	0.47105(54)	0.44216	1
O4	8c	0.2548(17)	0.15148(46)	0.23517(61)	0.35531	1
O5	8c	0.3546(12)	0.47919(54)	0.19406(61)	0.43426	1

TABLE V: The refined parameters of atomic coordinates (x , y , z), and site occupancy (*Occupancy*) obtained by the Rietveld refinement of the neutron diffraction pattern of BiYbGeO₅ taken at 50 mK using $\lambda = 2.41 \text{ \AA}$ incident wavelength.

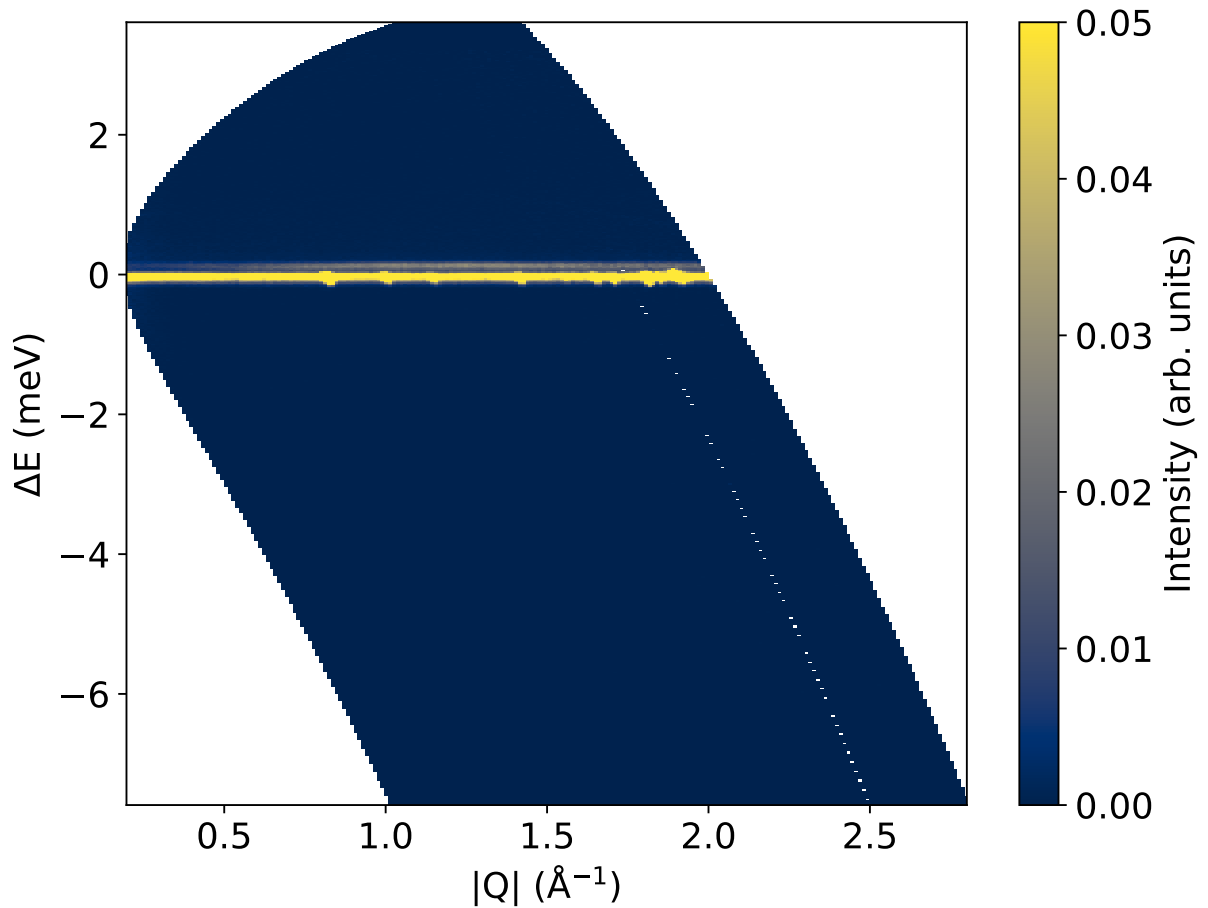


FIG. 6: A cut along ΔE made by subtracting the 100 K INS data from the 250 mK. This excitation has been fit to a Gaussian function, centered at 0.14 meV. The full width at half maximum for the Gaussian is 0.09 meV, which is comparable to the resolution of HYSPEC (~ 0.1 meV).

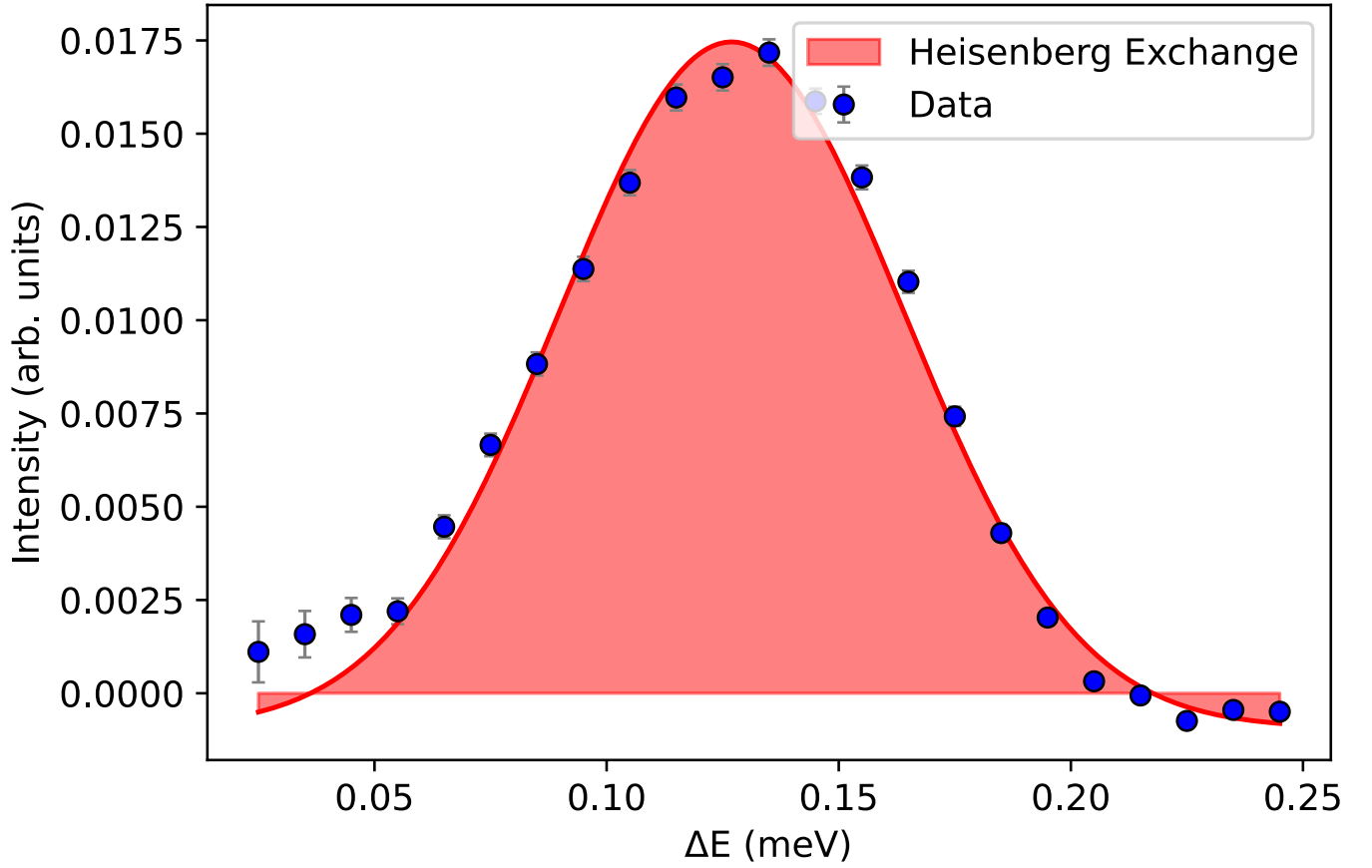


FIG. 7: A cut along ΔE made by subtracting the 100 K INS data from the 250 mK data. This excitation has been fit to a Gaussian function, centered at 0.13 meV. The full width at half maximum for the Gaussian is 0.09 meV, which is comparable to the resolution of HYSPEC (~ 0.1 meV).

Parameter	Gaussian
H	$-0.000925 \pm 8.17e - 05$
a	0.0184 ± 0.000164
b	0.127 ± 0.000333
c	0.0371 ± 0.000412
FWHM	≈ 0.09
χ^2	128.688

TABLE VI: Parameters for single Gaussian fit.

Parameter	Gaussian 1	Gaussian 2
H	-0.000614 ± 0.000111	
a	0.00829 ± 0.00977	0.0132 ± 0.00579
b	0.151 ± 0.00667	0.113 ± 0.0209
c	0.0249 ± 0.00595	0.0348 ± 0.00777
FWHM	≈ 0.08	≈ 0.06
χ^2	25.382	

TABLE VII: Parameters for double Gaussian fit.

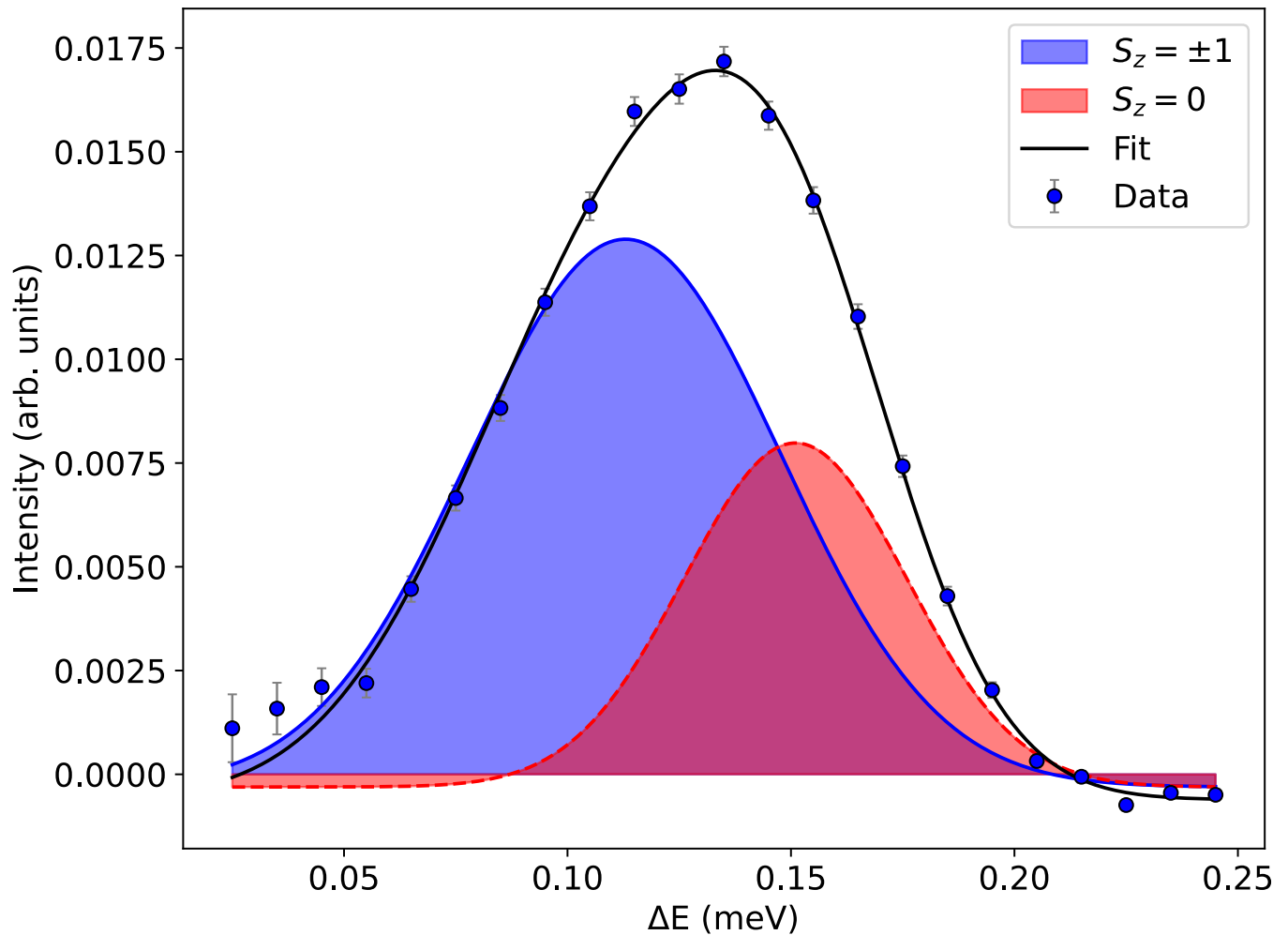


FIG. 8: A cut along ΔE made by subtracting the 100 K INS data from the 250 mK. This excitation has been fit to the sum of two Gaussians, centered at 0.11(2) meV and 0.15(1) meV, consistent with an XXZ-type intradimer exchange interaction. The full widths at half maximum for the Gaussians are 0.08 meV and 0.06 meV, respectively, which are smaller than the resolution of HYSPEC (~ 0.1 meV).

Parameter	Gaussian 1	Gaussian 2	Gaussian 3
H	$-0.000597 \pm 8.87e - 05$		
a	0.0079 ± 0.0446	0.014 ± 0.0523	0.00144 ± 0.00418
b	0.155 ± 0.0297	0.116 ± 0.0499	0.025 ± 0.332
c	0.0236 ± 0.0173	0.0317 ± 0.0669	0.0527 ± 1.62
FWHM	≈ 0.06	≈ 0.07	≈ 0.12
χ^2	16.470		

TABLE VIII: Parameters for triple Gaussian fit.

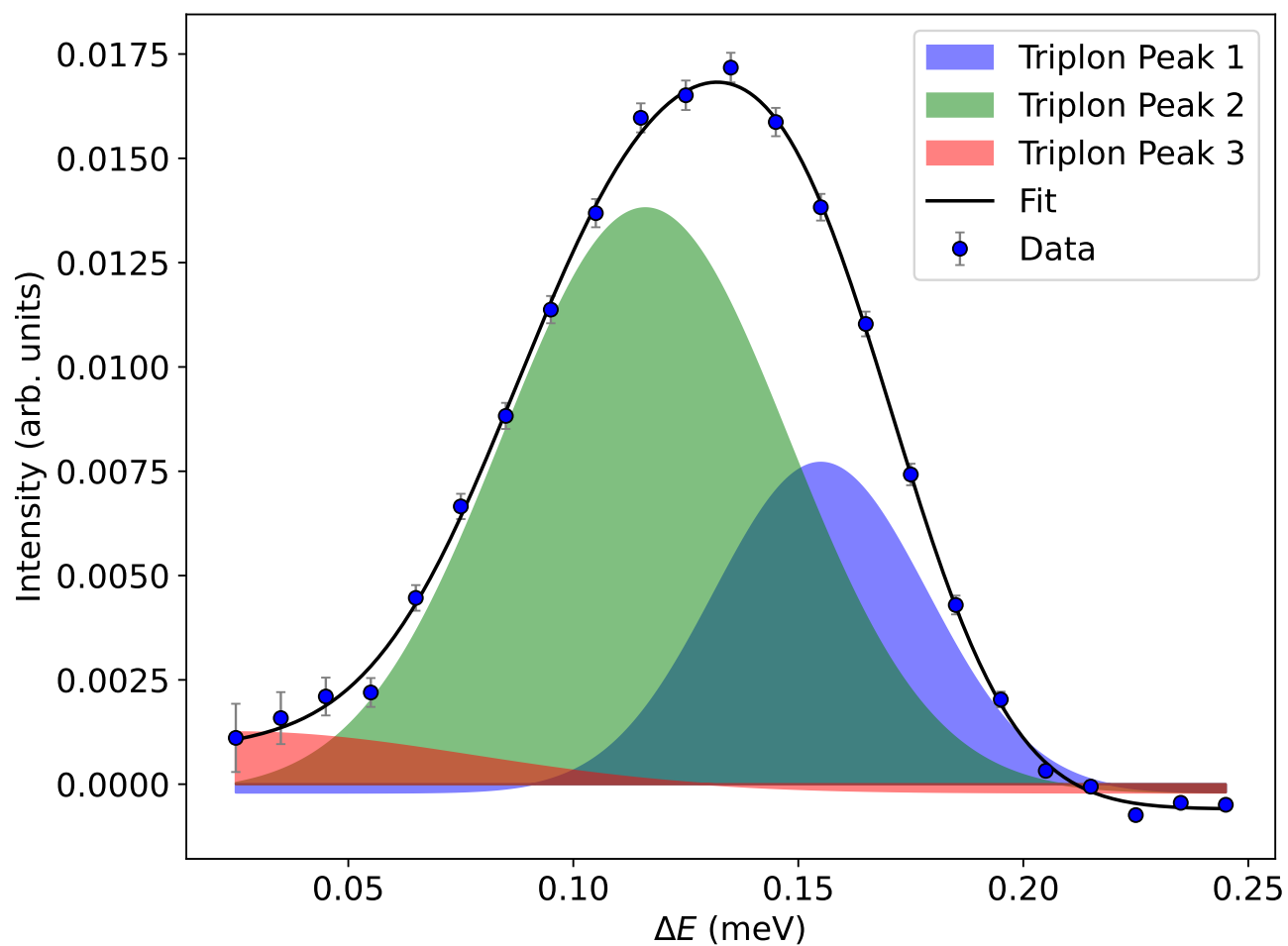


FIG. 9: A cut along ΔE made by subtracting the 100 K INS data from the 250 mK. This excitation has been fit to the sum of three Gaussians. The χ^2 shows this is an overfit with large errors in the fitted parameters. A very broad peak (in red) in the fitted Gaussian can be seen, which has a larger FWHM than the instrumental resolution.